High temperature characterization of double base epilayer 4H-SiC BJTs*

Zhang Qian(张倩)†, Zhang Yuming(张玉明), Zhang Yimen(张义门), and Wang Yuehu(王悦湖)

(Key Laboratory of Semiconductor Wide Band-Gap Materials and Devices, School of Microelectronics, Xidian University, Xi'an 710071, China)

Abstract: Based on the material characteristics and the operational principle of the double base epilayer BJTs, and according to the drift–diffusion and the carrier recombination theory, the common emitter current gain is calculated considering four recombination processes. Then its performance is analyzed under high temperature conditions. The results show that the emitter injection efficiency decreases due to an increase in the base ionization rate with increasing temperature. Meanwhile, the SiC/SiO_2 interface states and the quality of the passivation layer will affect the surface recombination velocity, and make an obvious current gain fall-off at a high collector current.

Key words: 4H-SiC; bipolar junction transistors (BJTs); current gain; carrier recombination; high temperature
DOI: 10.1088/1674-4926/31/11/114005 **PACC:** 7210; 7220; 7280

1. Introduction

With the increasing demand for devices of superior high-power, high-frequency performance and the ability to operate in rigorous environments, such as in high-temperature conditions, silicon carbide (SiC) has been recognized as one of the potential choices for application to different devices due to its high thermal conductivity (4.5 W/(cm·K)). In comparison with power MOSFETs, 4H-SiC bipolar junction transistors (BJTs) offer higher current densities at lower offset voltages, higher operating temperature and better reliability. In order to reduce the driving loss, the common-emitter current gain (β_{CE}) is very important among all of the performance parameters. Much work has been done to increase β by optimizing the emitter geometry[1, 2], by improving the passivation layer[3] and by improving the base epilayer process[4]. In our previous work, we put forward a novel structure of a bipolar transistor with double base epilayers[5]. This structure can not only avoid the ion implantation process but also reduce the base transit time. However, the temperature dependence of its working performance has not been unambiguously determined yet.

In the present work, we focus on the DC characteristics at an elevated temperature and calculated in terms of models including (1) surface recombination; (2) recombination in the emitter–base space charge region (SCR); and (3) incomplete ionization. Then the expression of β_{CE} is solved, and is validated by the two-dimensional simulation tools. The calculation results show that β_{CE} performs the negative temperature coefficient at elevated temperature. Also, the SiC/SiO_2 interface states and the quality of the passivation layer can affect the surface recombination velocity to decrease β_{CE}.

2. Device structure and modeling

A schematic cross-sectional view of the fabricated 4H-SiC BJTs is shown in Fig. 1. The base was grown as a two-layer structure with Al doping: 0.35 μm with 1×10^{17} cm^{-3}, followed by 0.15 μm with 4.6×10^{18} cm^{-3} on top. This configuration can accelerate the carriers by the built-in electric field in the base region and reduce the base transit time. Also, it can avoid the ion implantation process and reduce the defects introduced by the high-temperature annealing.

2.1. Physical models analysis

The physical models considered in this research include Shockley-Read-Hall (SRH) recombination, Auger recombination, surface-recombination mechanisms, mobility models and incomplete ionization models when carriers are injected from emitter transport through the base region. In the latter analysis, we ignore the bulk resistor of the semiconductor and the electrode contact resistance, and assume the base width constant, that is to say, we do not consider the Early effect, which is a good approximation for the low doped collector region.

2.1.1. SRH recombination

The interface states are located at the base-emitter junction and the SiC/SiO_2 interface, as shown in Fig. 1. Both of them recombine through deep levels in the bandgap. The SRH recombination rate R^{SRH} can be defined as

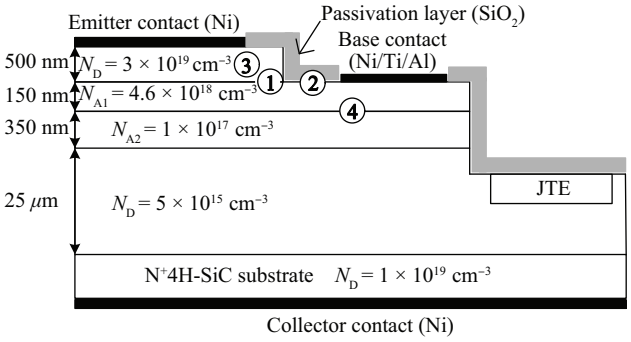

Fig. 1. Schematic structure of the NPN 4H-SiC BJTs.

* Project supported by the National Natural Science Foundation of China (No. 60876061) and the Key Laboratory Foundation of China (No. 20090C1403).

† Corresponding author. Email: zq_xacom@163.com

Received 24 May 2010, revised manuscript received 29 June 2010

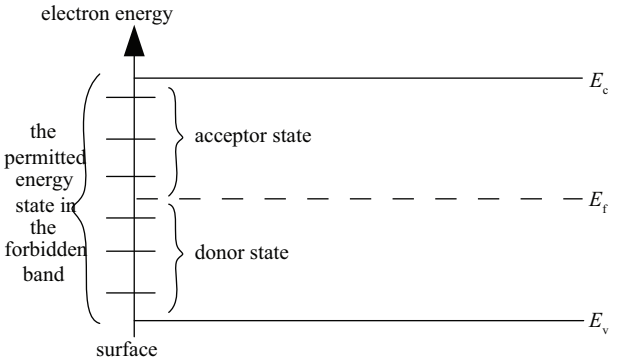

Fig. 2. Distribution of the surface state in the forbidden band.

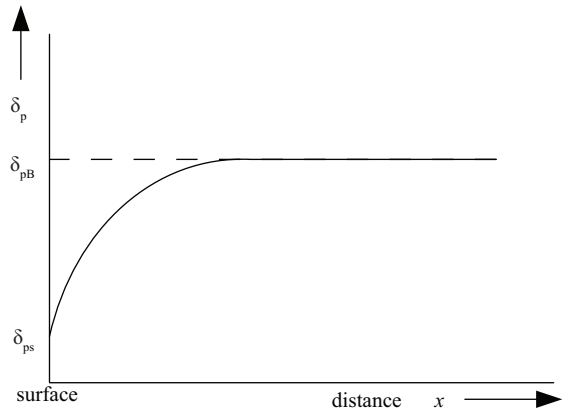

Fig. 3. Relationship between the excess carrier concentration and the surface distance.

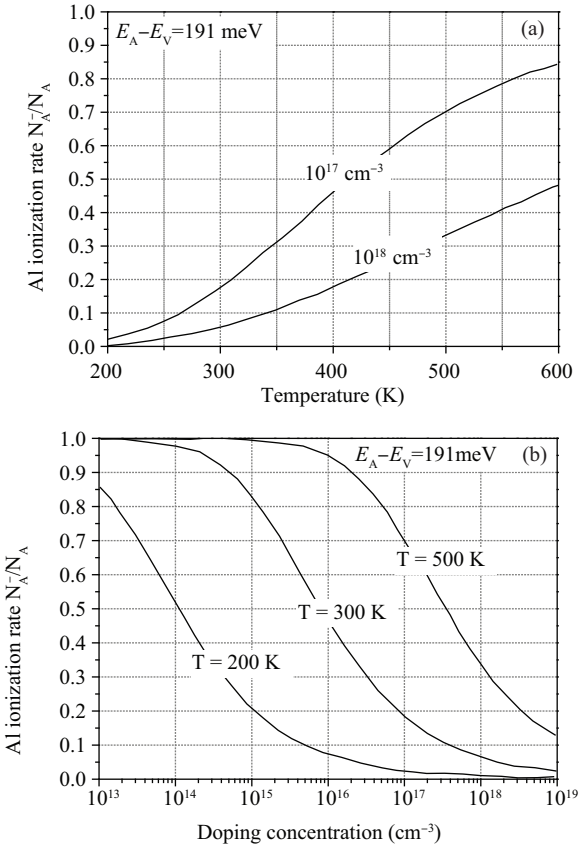

Fig. 4. Ionization rate of Al in 4H-SiC as a function of (a) doping concentration and (b) temperature.

$$R^{\mathrm{SRH}} = \frac{np - n_{\mathrm{i}}^2}{\tau_{\mathrm{p}}\left(n + n_{\mathrm{i}} \exp\dfrac{E_{\mathrm{trap}}}{kT}\right) + \tau_{\mathrm{n}}\left(p + n_{\mathrm{i}} \exp\dfrac{-E_{\mathrm{trap}}}{kT}\right)}, \tag{1}$$

where τ_{n} and τ_{p} are the electron and hole lifetimes, which depend on temperature, dopant type and defect concentration. They are in the range of 0.1–2 μs. In our calculation process, we assume $\tau_{\mathrm{n}} = 5\tau_{\mathrm{p}}$.

2.1.2. Auger recombination

Auger recombination is important at high carrier concentrations. The band-to-band Auger recombination rate R_{A} is given by

$$R_{\mathrm{A}} = (C_{\mathrm{n}} n + C_{\mathrm{p}} p)(np - n_{\mathrm{i}}), \tag{2}$$

where C_{n} and C_{p} denote the Auger coefficients of electrons and holes. For 4H-SiC, $C_{\mathrm{n}} = 5\times10^{-31}$ cm^{-6}·s^{-1}, $C_{\mathrm{p}} = 2\times10^{-31}$ cm^{-6}·s^{-1}[6].

2.1.3. Surface recombination

As Figure 2[7] shows, there exists the distribution of the permitted energy states in the forbidden band region. It can be proved that the defect density at the device surface is larger than that in the bulk of the material. Therefore, as Figure 3[7] shows, the excess carrier in the material will diffuse from the interior to the surface. For an extrinsic semiconductor, the surface recombination rate can be expressed as

$$R_{\mathrm{s}} = \frac{\delta_{\mathrm{ps}}}{\tau_{\mathrm{p0s}}}, \tag{3}$$

where τ_{p0s} is the lifetime and δ_{ps} is the concentration of the excess minority carrier located at the surface.

2.1.4. Incomplete ionization

Unlike Si, the donor (E_{D}) and acceptor (E_{A}) levels in SiC are relatively deep compared to the thermal energy at room temperature, so the dopants in SiC are not fully ionized, even at high temperature. The concentration of the ionized impurity atoms is given by[8]

$$\begin{cases} N_{\mathrm{D}}^{+} = \dfrac{N_{\mathrm{D}}}{1 + g_{\mathrm{c}} \exp\dfrac{E_{\mathrm{Fn}} - E_{\mathrm{D}}}{kT}}, \\ N_{\mathrm{A}}^{-} = \dfrac{N_{\mathrm{A}}}{1 + g_{\mathrm{v}} \exp\dfrac{E_{\mathrm{A}} - E_{\mathrm{Fp}}}{kT}}, \end{cases} \tag{4}$$

where N_{D} and N_{A} are the doping concentrations of the donor and acceptor, and E_{D} and E_{A} are the donor and acceptor energy level, respectively. For nitrogen donor levels in 4H-SiC, a dopant ionization energy $E_{\mathrm{C}} - E_{\mathrm{D}} = 65$ meV and $g_{\mathrm{c}} = 2$, the p-type doping can be achieved with Al acceptors with ionization energy $E_{\mathrm{A}} - E_{\mathrm{V}} = 191$ meV[9] and $g_{\mathrm{v}} = 4$. Figure 4[10]

shows the ionization rate of Al in 4H-SiC as a function of doping concentration and temperature. From this figure we can see that the Al ionization rate increases with increasing temperature and decreasing doping concentration.

2.2. Common-emitter current gain

The common-emitter current gain β_{CE} is an important parameter that is defined as the ratio of the collector current density and the base current density. In order to indicate the influence of the temperature on β_{CE}, the following recombination mechanism is taken into account: (1) recombination in the emitter junction space charge region (SCR); (2) surface recombination; (3) recombination in the emitter; and (4) recombination in the double base epilayer, as shown in Fig. 1.

The current gain β_{CE} can be expressed as

$$\beta_{CE}^{-1} = \beta_{SCR}^{-1} + \beta_{sr}^{-1} + \beta_{E}^{-1} + \beta_{T}^{-1}. \tag{5}$$

The recombination current density J_{SCR} caused by the recombination in the SCR of the emitter junction is given by

$$J_{SCR} = j_{or} \exp \frac{qV_{BE}}{2kT}, \tag{6}$$

where j_{or} is the recombination saturation current, q is the electron charge and V_{BE} is the external voltage across the BE junction.

The emitter current density J_E can be expressed as

$$J_E = j_{od} \exp \frac{qV_{BE}}{kT}, \tag{7}$$

$$j_{od} = \frac{qD_{nB}n_B^0}{W_B}, \tag{8}$$

where D_{nB} is the diffusion coefficient of the minority carrier in the base and n_B^0 is the equilibrium electron density in the p-base.

Combining Eqs. (6)–(8), β_{SCR} is expressed as

$$\beta_{SCR}^{-1} = \frac{J_{SCR}}{J_E} = \frac{j_{or}}{j_{od} \exp \dfrac{qV_{BE}}{2kT}} = \frac{j_{or}}{\sqrt{j_E j_{od}}}. \tag{9}$$

Secondly, β_{sr} is the current gain related to the surface recombination and it is defined as

$$\beta_{sr}^{-1} = \frac{J_{sr}}{J_{nE}}, \tag{10}$$

$$J_{sr} = qs \frac{n_i^2 \exp \dfrac{qV_{BE}}{kT}}{N_B(0)}, \tag{11}$$

$$J_{nE} = \frac{qsn_i^2}{Q_B} \exp \frac{qV_{BE}}{kT}, \tag{12}$$

$$Q_B = \int_0^{W_B} N_B(x)\mathrm{d}x, \tag{13}$$

$$N_B(x) = \begin{cases} N_1, & 0 < x < W_a, \\ N_2, & W_a < x < W_B. \end{cases} \tag{14}$$

Combining Eqs. (10)–(14), β_{sr} is described as

$$\beta_{sr}^{-1} = \frac{sQ_B}{D_{nB}N_{B(0)}}, \tag{15}$$

where s is the surface recombination velocity.

Thirdly, β_E is limited by the decrease in the injection coefficient at high-injection levels and is given by[11]

$$\beta_E^{-1} = \frac{J_{pd}}{J_E} \approx \frac{D_{pE} j_E W_B^2}{qD_a^2 N_E L_{pE}}, \tag{16}$$

where D_{pE} and L_{pE} are the hole diffusion coefficient and hole diffusion length in the emitter, and D_a is the ambipolar carrier diffusion coefficient in the base, which can be expressed by

$$D_a = \frac{2D_{nB}D_{pB}}{D_{nB} + D_{pB}}. \tag{17}$$

Finally, β_T is defined as the ratio of the electron current density injected into the base region from the emitter junction with recombination current density in base region, as shown by

$$\beta_T^{-1} = \frac{J_{vB}}{J_{nE}}. \tag{18}$$

J_{vB} is calculated by Eq. (18) due to a built-in electrical field existing in the base region, which consists of two epilayers with different doping concentrations,

$$J_{vB} = \frac{q}{\tau_{nB}} \int_0^{W_B} \Delta n_B(x)\mathrm{d}x = \frac{q}{\tau_{nB}} \int_0^{W_B} \left[n_B(x) - n_B^0\right] \mathrm{d}x, \tag{19}$$

where $n_B(x)$ is the minority-carrier concentration profile in the base. When neglecting n_B^0 and substituting the expression of $n_B(x)$[5] into Eq. (18), the recombination current in the base is obtained,

$$\begin{aligned} J_{vB} =& \frac{q}{\tau_{nB}} \frac{I_{nE}}{qD_{nB}} \int_0^{W_B} n_B(x)\mathrm{d}x \\ =& \frac{I_{nE}}{\tau_{nB}D_{nB}} \int_0^{W_B} \left[\frac{1}{N_B(x)} \int_x^{W_B} N_B(x)\mathrm{d}x \right] \mathrm{d}x \\ =& \frac{I_{nE}}{L_{nB}^2} \left[\frac{1}{2}L_1^2 + \frac{N_2}{N_1}L_1L_2 + \frac{N_1}{N_2}L_2\left(L_1 - \frac{1}{2}L_2\right) \right. \\ & \left. + L_2^2 \right] \left[\frac{W_a}{N_1} + \frac{W_B - W_a}{N_2} \right], \end{aligned} \tag{20}$$

where N_1 and N_2 are the doping concentrations of the P^+ and P layer, $L_1 = W_a$ and $L_2 = W_B - W_a$.

3. Results and discussions

The temperature dependent DC performance is calculated using the models outlined above with the help of the DESSIS-ISE software. The material and device parameters used in the calculation are summarized in Table 1.

In order to validate the correction of the calculation model, a simulation for a device that has only one base epilayer is made to compare with the measured results. Figure 5 shows a comparison of the experimental[13] and simulation results at T =

Table 1. Material and device parameters used in the calculation.

	Parameter	Value
Device parameter	Emitter doping concentration/thickness	3×10^{19} cm^{-3}/0.5 μm
	Base doping concentration/thickness (top)	4.6×10^{18} cm^{-3}/0.15 μm
	Base doping concentration/thickness (bottom)	1×10^{17} cm^{-3}/0.35 μm
	Collector doping concentration/thickness	5×10^{15} cm^{-3}/25 μm
Material parameter	Bandgap energy (E_g)	3.26 eV
	Donor energy level	0.065 eV
	Acceptor energy level	0.191 eV
	μ_n	1110 cm^2/(V·s)[12]
	μ_p	65 cm^2/(V·s)
	Surface recombination velocity	2×10^6 cm/s

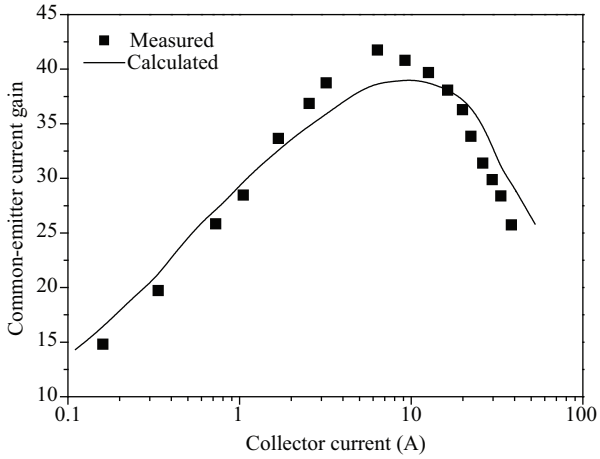

Fig. 5. Comparison of CE current gain as a function of the collector current of the experimental and simulation results.

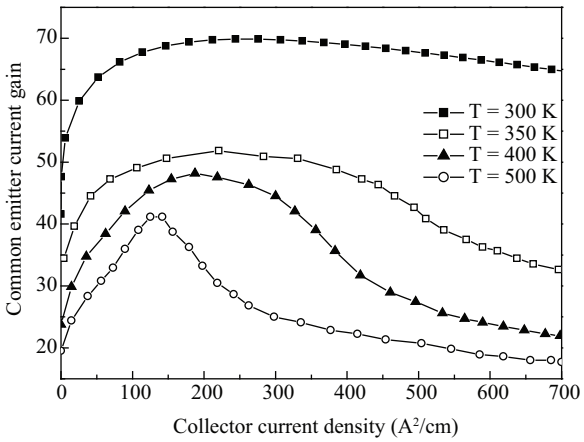

Fig. 7. CE current gain versus collector current density at different temperatures.

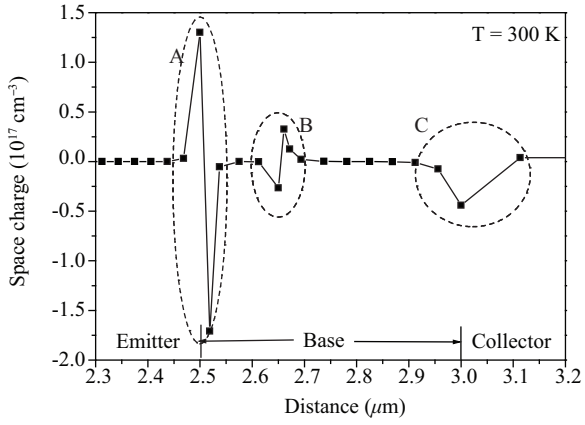

Fig. 6. Space charge profile in the base region at room temperature.

300 K. It shows that the presented model for calculation is reasonable.

Figure 6 illustrates the space charge profile in the base region at room temperature. In this figure, it can be seen that there exists a space charge region in the bulk of the base. The P^+ side is negative charge and the P side is the accumulation of the hole carrier, which has no obvious boundary. Also, we can find that the Al dopants in the base region are not fully ionized. The hole concentration will grow with increasing temperature, which will strongly affect the emitter-injection efficiency and base transport factor.

Figure 7 shows the dependences of the common-emitter current gain β_{CE} on the collector current density at four different temperatures. With increasing temperature, the ionization rate of the Al dopants in the base region increase and they cause a substantial decrease in emitter injection efficiency. Therefore, the common-emitter current gain decreases rapidly at a higher temperature. Overall, the current gain decreases rapidly at a higher temperature. This is very different from power silicon BJTs and makes the device attractive for paralleling and thermal run-away suppression. Figure 8 illustrates the temperature dependence of the common-emitter current gain. As Figure 7 shows, β_{CE} performs the negative temperature coefficient.

Figure 9 shows the forward I–V characteristics at room temperature and together with those at T = 500 K. From this figure it is observed that there is an obvious degradation in the device performance at elevated temperature. That is mainly because, with increasing temperature, the surface recombination at the SiC/SiO_2 interface becomes aggravating, which ultimately increases the SRH recombination rate and base recombination current. This confirms that the SiC/SiO_2 interface plays an important role in the BJT's performance. Thus, an improvement in the passivation layer quality is necessary.

Figure 10 shows the DC current gain over a wide range of emitter–base voltage for the transistors with two different temperatures, while the collector–base voltage is kept constant

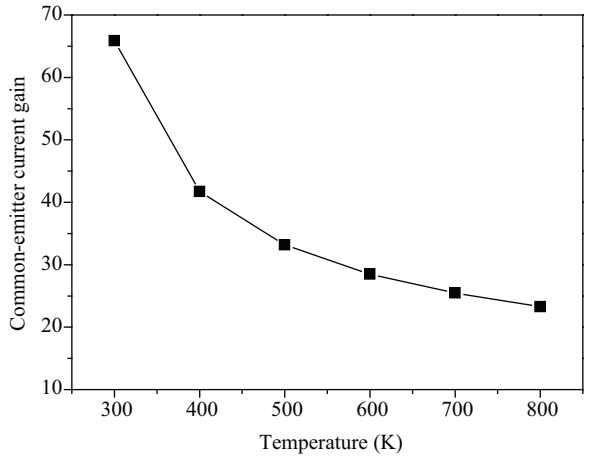

Fig. 8. Temperature dependence of the common-emitter current gain.

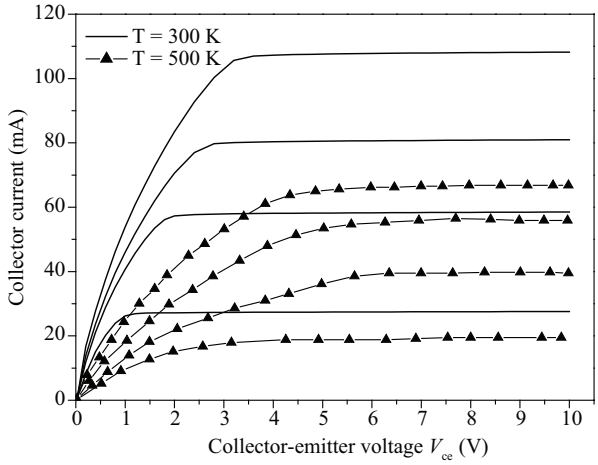

Fig. 9. Forward I–V characteristics at room temperature and at T = 500 K.

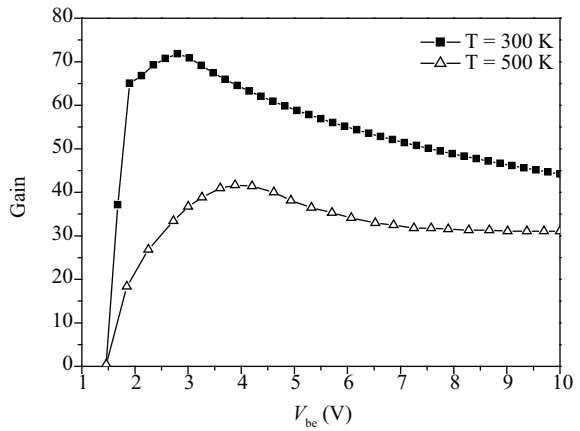

Fig. 10. Simulated current gain as a function of the emitter–base bias at different temperatures. V_{ce} is kept at a constant voltage of 6 V.

at 6 V. With increasing temperature, the maximum current gain decrease is from 70 to about 40.

4. Conclusion

The high-temperature performance of a double base epilayer 4H-SiC BJT is demonstrated in this paper. By solving the analytical expression of the common-emitter current gain considering recombination process, the β_{CE}–I_C dependences are determined at elevated temperature based on models including recombination, incomplete ionization, bandgap narrowing and a built-in field in the base region. The simulation results show that the current gain has a negative temperature coefficient. This makes the device attractive for paralleling and thermal runaway suppression. Meanwhile, the SiC/SiO_2 interface states and the quality of the passivation layer will affect the surface recombination velocity, and make a current gain fall-off at a high collector current.

References

[1] Domeij M, Lee H S, Danielsson E, et al. Geometrical effects in high current gain 1100-V 4H-SiC BJTs. IEEE Electron Device Lett, 2005, 26(10): 743

[2] Zhang J H, Li X Q, Alexandrov P, et al. Fabrication and characterization of high-current-gain 4H-SiC bipolar junction transistors. IEEE Trans Electron Devices, 2008, 55(5): 1899

[3] Lee H S, Domeij M, Zetterling C M, et al. 1200-V 5.2-m$\Omega\cdot$cm^2 4H-SiC BJTs with a high common-emitter current gain. IEEE Electron Device Lett, Nov 2007, 28(11):1007

[4] Lee H S, Domeij M, Ghandi R, et al. High-current-gain SiC BJTs with regrown extrinsic base and etched JTE. IEEE Trans Electron Devices, 2008, 55(8): 1894

[5] Zhang Qian, Zhang Yuming, Zhang Yimen. Analytical models for the base transit time of a bipolar transistor with double base epilayers. Journal of Semiconductors, 2009, 30(9): 094003

[6] Galeckas A, Linnros J, Grivickas V, et al. Auger recombination in 4H-SiC: unusual temperature behavior. Appl Phys Lett, 1997, 71: 3269

[7] Neamen D A. Semiconductor physics and devices. 3rd ed. Beijing: Publishing House of Electronics Industry, 2007: 160

[8] Troffer T, Schadt M, Frank T, et al. Doping of SiC by implantation of boron and aluminum. Phys Status Solidi A, 1997, 162: 277

[9] Bakowski M, Gustafsson U, Lindefelt U. Simulation of SiC high power devices. Phys Status Solidi A, 1997, 162: 421

[10] Li X. Design and simulation of high voltage 4H silicon carbide power devices. PhD Thesis, New Burnswick Rutgers, the State University of New Jersey, 2005

[11] Han Ru, Li Cong, Yang Yintang, et al. Analysis of early voltage in 4H-SiC BJTs. Chinese Journal of Semiconductors, 2007, 28(9): 1433

[12] Joshi R P. Monte Carlo calculation of the temperature and field dependent electron transport parameters for 4H-SiC. J Appl Phys, 1995, 78(9): 5518

[13] Ivanov P A, Levinshtein M E, Agarwal A K, et al. Temperature dependence of the current gain in power 4H-SiC NPN BJTs. IEEE Trans Electron Devices, 2006, 53(5): 1245